Circulation Research

ORIGINAL RESEARCH

Multiscale Analysis of Extracellular Matrix Remodeling in the Failing Heart

Ana Rubina Perestrelo, Ana Catarina Silva, Jorge Oliver-De La Cruz, Fabiana Martino, Vladimír Horváth, Guido Caluori, Ondřej Polanský, Vladimír Vinarský, Giulia Azzato, Giuseppe de Marco, Víta Žampachová, Petr Skládal, Stefania Pagliari, Alberto Rainer, Perpétua Pinto-do-Ó, Alessio Caravella, Kamila Koci, Diana S. Nascimento, Giancarlo Forte

RATIONALE: Cardiac ECM (extracellular matrix) comprises a dynamic molecular network providing structural support to heart tissue function. Understanding the impact of ECM remodeling on cardiac cells during heart failure (HF) is essential to prevent adverse ventricular remodeling and restore organ functionality in affected patients.

OBJECTIVES: We aimed to (1) identify consistent modifications to cardiac ECM structure and mechanics that contribute to HF and (2) determine the underlying molecular mechanisms.

METHODS AND RESULTS: We first performed decellularization of human and murine ECM (decellularized ECM) and then analyzed the pathological changes occurring in decellularized ECM during HF by atomic force microscopy, 2-photon microscopy, high-resolution 3-dimensional image analysis, and computational fluid dynamics simulation. We then performed molecular and functional assays in patient-derived cardiac fibroblasts based on YAP (yes-associated protein)-transcriptional enhanced associate domain (TEAD) mechanosensing activity and collagen contraction assays. The analysis of HF decellularized ECM resulting from ischemic or dilated cardiomyopathy, as well as from mouse infarcted tissue, identified a common pattern of modifications in their 3-dimensional topography. As compared with healthy heart, HF ECM exhibited aligned, flat, and compact fiber bundles, with reduced elasticity and organizational complexity. At the molecular level, RNA sequencing of HF cardiac fibroblasts highlighted the overrepresentation of dysregulated genes involved in ECM organization, or being connected to TGFβ1 (transforming growth factor β1), interleukin-1, TNF-α, and BDNF signaling pathways. Functional tests performed on HF cardiac fibroblasts pointed at mechanosensor YAP as a key player in ECM remodeling in the diseased heart via transcriptional activation of focal adhesion assembly. Finally, in vitro experiments clarified pathological cardiac ECM prevents cell homing, thus providing further hints to identify a possible window of action for cell therapy in cardiac diseases.

CONCLUSIONS: Our multiparametric approach has highlighted repercussions of ECM remodeling on cell homing, cardiac fibroblast activation, and focal adhesion protein expression via hyperactivated YAP signaling during HF.

GRAPHIC ABSTRACT: A graphic abstract is available for this article.

Key Words: cardiomyopathy, dilated ■ elasticity ■ extracellular matrix ■ fibroblasts

Editorial, see p 39 | In This Issue, see p 2 | Meet the First Author, see p 3

Heart diseases present with varied cause, symptoms, and progression, but they all result in the reduced pumping efficiency of the organ. This occurs because of cardiomyocyte death and replacement of healthy heart tissue with noncompliant, akinetic scar-like tissue, in a process-dubbed ECM (extracellular matrix) remodeling.[1] Although cardiac fibroblast (CF) activation and ECM remodeling prevent the initial rupture of the ventricular

Correspondence to: Ana Rubina Perestrelo, International Clinical Research Center, St. Anne's University Hospital, Studentská 6, 62500 Brno, Czech Republic, Email anarubiperestrelo@gmail.com or Giancarlo Forte, International Clinical Research Center, St. Anne's University Hospital, Studentská 6, 62500 Brno, Czech Republic, Email giancarlo.forte@fnusa.cz

The Data Supplement is available with this article at https://www.ahajournals.org/doi/suppl/10.1161/CIRCRESAHA.120.317685.

For Sources of Funding and Disclosures, see page 37.

Novelty and Significance

What Is Known?

- Remodeling of the ECM (extracellular matrix) parallels and exacerbates the impact of cardiac diseases.
- Pathological remodeling of the ECM is associated with a switch in its protein composition.

What New Information Does This Article Contribute?

- This study identifies reproducible modifications to ECM structure and mechanics that contribute to heart failure.
- These modifications are sufficient to induce cardiac fibroblast activation and affect cell homing per se.
- Cardiac fibroblast activation is mediated by the mechanosensing protein YAP (yes-associated protein), which eventually exacerbates ECM remodeling.

For the first time, a multiscale and multiparametric strategy based on human heart tissue decellularization, atomic force, 2-photon microscopy, and computational fluid dynamics simulation was used to define a common pattern of modifications in ECM 3-dimensional structure and mechanical properties. These changes were found to be consistent and reproducible in cardiac pathologies with different cause. We demonstrate that mechanical cues arising from pathological ECM are sufficient to activate the YAP mechanosensitive protein in cardiac fibroblast cell lines generated from patients. In turn, the activation of YAP takes part in the remodeling of the ECM itself, thereby forming a positive loop.

Nonstandard Abbreviations and Acronyms

α-SMA	α-smooth muscle actin
CF	cardiac fibroblast
CFD	computational fluid dynamics
CTGF	connective tissue growth factor
DCM	dilated cardiomyopathy
dECM	decellularized ECM
ECM	extracellular matrix
HF	heart failure
IHD	ischemic heart disease
MI	myocardial infarction
SHG	second harmonic generation
TEAD	transcriptional enhanced associate domain
TGFβ1	transforming growth factor β 1
YAP	yes-associated protein

wall, they eventually fuel a feed-forward profibrotic mechanism through which cardiac function is progressively impaired, ultimately resulting in heart failure (HF).[2] The knowledge of in-depth ECM composition, arrangement, and remodeling and its effect on cardiac cell function during heart disease is limited.[3] Thus, quantifying the composition, structure, and turnover of the ECM will be helpful to overcome the suboptimal translational models of ECM remodeling and possibly develop new therapeutics for disease treatment (ie, ECM-targeted antifibrotic drugs).

The heart exhibits extraordinary 3-dimensional (3D) complexity and comprises highly specialized contractile cells. Mimicking the geometry and function of native heart tissue to fabricate artificial substitutes to be used as clinically relevant in vitro disease models or constructs to be implanted in vivo is a major challenge.

Decellularization describes a process by which the cells are removed from the tissue, leaving behind the intact ECM scaffold. Recent decellularization protocols have provided a toolbox to visualize the 3D organization, mechanical properties, and chemical complexity of the cardiac ECM[4] and its remodeling during cardiac pathologies.[5] Such studies on ECM pathological remodeling have mostly focused on characterizing the changes in ECM biochemical composition. In this case, tissue decellularization is typically followed by lyophilization and digestion, resulting in loss of the native 3D geometric information.[6] Cardiac ECM remodeling has been thoroughly investigated in rodent models through this approach; here, collagen deposition, fibronectin turnover, and laminin reduction, as well as impaired ECM compliance have been described.[7]

Despite these advances, how activated CFs contribute to modify ECM structure and stiffness in patients remains largely unknown. Recent studies by our group and others disclosed that the mechanosensitive YAP (yes-associated protein) is activated after myocardial infarction (MI) in mice.[8,9] Interestingly, we recently discovered that YAP is activated by 3D ECM organization[10] and acts as the main regulator of cell-matrix interactions by contributing to focal adhesion protein assembly.[11] YAP transcriptional activity has also been implicated in cancer ECM remodeling,[12] but its potential role in HF-associated ECM turnover is unknown.

Here, we combined recent advances in ECM decellularization protocols with multimodality imaging and functional studies to define key physical features in patient-derived HF ECM, and to identify the effects of altered ECM architecture on CFs in vitro. We investigated the effect of HF-associated ECM remodeling on CF gene expression and propose a role for YAP mechanosensor in pathological ECM remodeling in heart disease.

METHODS

Data Availability

All data and materials have been made publicly available (Table).

Patient-Derived Heart Tissue Collection

Human healthy and diseased heart left ventricle apexes were obtained from cadaveric donors of nontransplantable hearts (N=4), routine surveillance endomyocardial biopsies (N=3) post-transplantation, and from cardiac patients diagnosed with dilated cardiomyopathy (DCM, N=18) or ischemic heart disease (IHD, N=12) that underwent ventricular assist device implantation or transplantation (see patient details in Online Table I). All experiments were performed in accordance with the ethical standards of the Centre of Cardiovascular and Transplantation Surgery and approved by the Ethics Committee of St. Anne's University Hospital, Brno, Czech Republic.

MI Mouse Model

MI was experimentally induced by ligating the left anterior descending coronary artery in C57BL/6 adult mice (9–10 weeks), as previously described.[13] Mice hearts cohort was composed of 4 days post-MI (acute MI, N=7), 21 days post-MI (chronic MI, N=7), sham-operated (no ligation of the coronary artery, 4- and 21-days post-surgery, N=6), and nonoperated (N=4) controls (Online Figure IB). All animal experiments were approved by the local Ethics Committees. See the Data Supplement for details.

Cardiac Tissue Decellularization and Characterization

Decellularized ECMs (dECMs) were generated from human and murine specimens as previously described,[14,15] with minor modifications (Data Supplement). Human heart tissues were received at our facility by an operator, who was not informed about the nature of the sample. The analysis was independently performed by 2 blind operators. The apical region of the left ventricle was analyzed across the myocardium thickness. See the Data Supplement for details on biochemical (total collagen quantification and mass spectrometry), structural (multiphoton microscopy), topographical (scanning electron microscopy), and mechanical (atomic force microscopy) characterization of dECMs.

Table. RNA-Seq Data Availability

Description	Gene Expression Omnibus (GEO) repository
CTL CFs–CFs from healthy donor rep1	GSM4705298
CTL CFs–CFs from healthy donor rep2	GSM4705299
CTL CFs–CFs from healthy donor rep3	GSM4705300
DCMA CFs–CFs from DCM patient A rep1	GSM4705301
DCMA CFs–CFs from DCM patient A rep2	GSM4705302
DCMA CFs–CFs from DCM patient A rep3	GSM4705303
DCMB CFs–CFs from DCM patient B rep1	GSM4705304
DCMB CFs–CFs from DCM patient B rep2	GSM4705305
DCMB CFs–CFs from DCM patient B rep3	GSM4705306
CTL CFs YAP 8SA–CFs from healthy donor overexpressing YAP rep1	GSM4705307
CTL CFs YAP 8SA–CFs from healthy donor overexpressing YAP rep2	GSM4705308
CTL CFs YAP 8SA–CFs from healthy donor overexpressing YAP rep3	GSM4705309

CF indicates cardiac fibroblast; DCM, dilated cardiomyopathy; and YAP, yes-associated protein.

Image Analysis

The dECM structure was investigated using a computational fluid dynamics (CFD) approach to precisely characterize the geometric properties and spatial orientation of its fibers. See the Data Supplement for CFD modeling and simulation set up and Online Table III for image rendering, analysis, and quantification details.

Human Cardiac Fibroblast Derivation and Culture

Patient-derived primary CFs (N=6) were isolated by explant outgrowth on pregelatinized plates and sorted for a Thy1 (CD90)-positive and PECAM-1 (CD31)-negative population. Transcriptional enhanced associate domain (TEAD) reporter and YAP overexpression stable CF lines, gene and protein expression profiling (RNA sequencing, quantitative real-time PCR, Western Blotting, mass spectrometry), TGFβ1 (transforming growth factor β 1) stimulation, 3D cultures, and collagen contraction assays are detailed in the Data Supplement.

Please refer to the Major Resources Table in the Data Supplement for additional details.

RESULTS

Reduced Organ Function During HF Correlates With a Derangement in Myocardium Microstructure

The remodeling of ECM structure during the progression of cardiac diseases determines dramatic changes in its biochemical composition, topography, and mechanophysical properties.[16] With the aim of investigating HF ECM organization and microstructure, we grouped patients with HF according to their medical history (DCM, IHD) and recruited patients based on ejection fraction <40% and New York Heart Association Functional Classification Class III to IV (Figure 1A, Online Table I). Most patients (90%) were male, aged 30 to 68 years, with ejection fraction <20%, permanent arrhythmias, and cardiac decompensation, indicative of advanced HF (Online Table I).

Histological analysis of the explanted DCM and IHD hearts stained with Masson's trichrome confirmed microstructure derangement and increased collagen content—well-established markers of late cardiac disease[17] (Figure 1B). DCM and IHD hearts, however, exhibited different histological features (Online Figure IA): IHD hearts displayed characteristic scattered scar-like foci consistent with the interstitial fibrosis and calcifications,

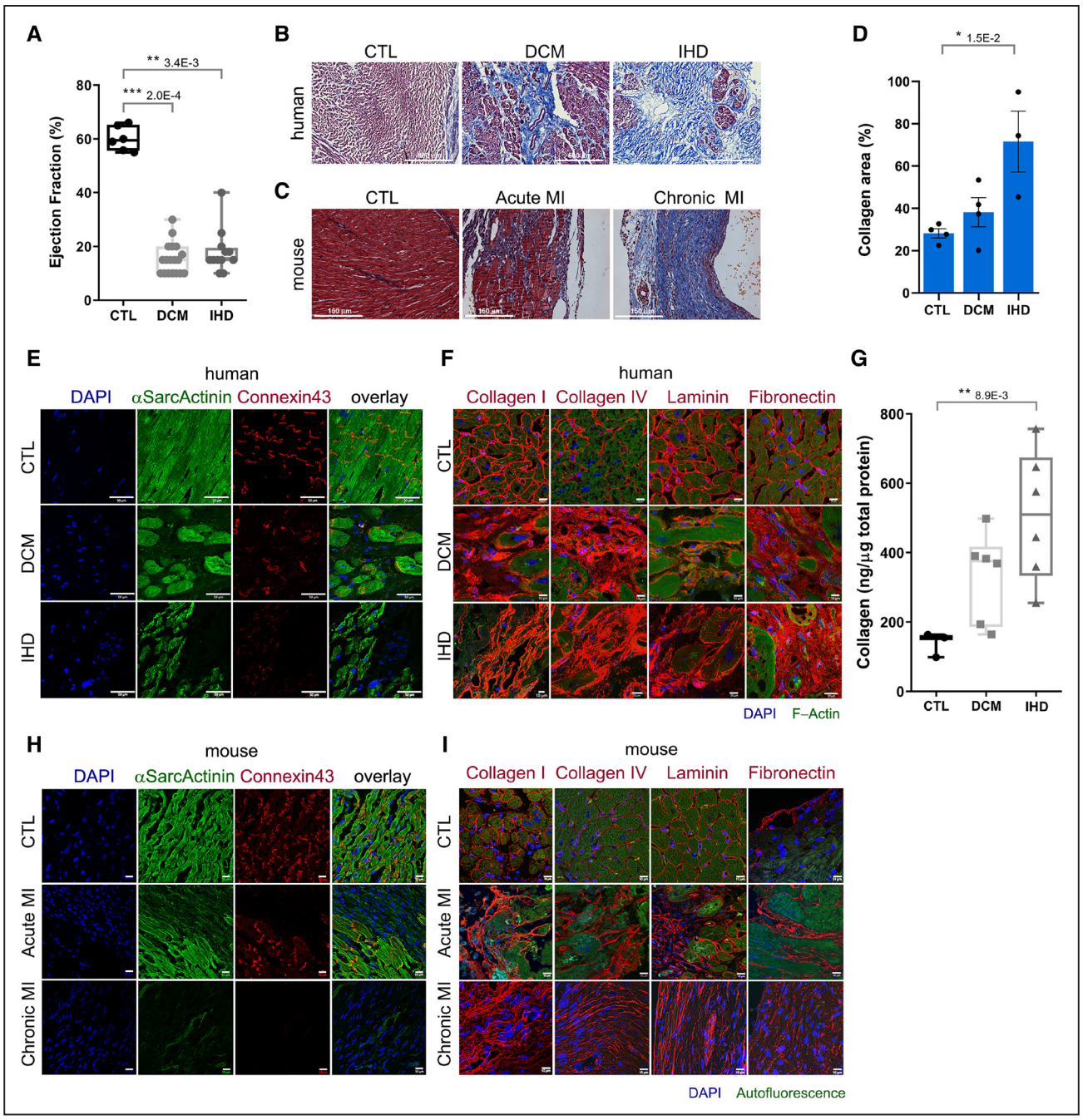

Figure 1. Deranged tissue microstructure underlies heart failure.
A, Ejection fraction evaluation in the patients enrolled in the study. Healthy (CTL, N=6), dilated cardiomyopathy (DCM, N=18), and ischemic heart disease (IHD, N=12); Kruskal-Wallis followed by Dunn tests. **B**, Representative Masson's trichrome staining of CTL, DCM, and IHD heart specimens. **C**, Masson's trichrome staining of murine heart specimens obtained after acute and chronic myocardial infarction (MI). CTL=sham-operated. **D**, Histopathologic evaluation of Masson's trichrome staining by the % collagen (blue) and muscle (red) staining on the total tissue area. CTL (N=4), DCM (N=4), IHD (N=3); Kruskal-Wallis followed by Dunn tests. **E** and **F**, Representative confocal microscopy images of CTL, DCM, and IHD heart specimens stained for the indicated cardiac and ECM (extracellular matrix) proteins. F-actin (green), nuclei (blue). Scale bar=50 and 10 µm, respectively. **G**, Absolute quantification of collagen composition in CTL, DCM, and IHD human hearts. CTL (N=3; n=2), DCM (N=6; n=2), IHD (N=6; n=2); Kruskal-Wallis followed by Dunn tests. **H** and **I**, Representative images of CTL, acute and chronic MI murine hearts stained for the indicated cardiac and ECM proteins. Scale bar=10 µm. Boxplots represent median±min/max and barplots represent mean±SD.

although DCM hearts presented with a characteristic diffuse fibrosis. We also analyzed murine heart tissues after inducing acute and chronic MI, a model of IHD. These tissues exhibited deranged features similar to human diseased hearts (Figure 1C) and were thus used as a reference throughout the study.

A significant 2.5-fold increase in fibrotic area in IHD compared with healthy hearts was confirmed as

a percentage of the collagen-positive surface area in human hearts (Figure 1D, Online Figure IA). Immunohistochemical staining for α-sarcomeric actinin and connexin-43 was then used to identify sarcomeric and homologous cell-cell electromechanical coupling, respectively. This analysis confirmed the loss of contractile cardiomyocytes in both IHD and DCM hearts, which exhibited tissue disorganization and decompaction (Figure 1E). We corroborated the impairment in tissue integrity by analyzing structural ECM proteins—collagen I (fibril-forming collagen), collagen IV (network-forming collagen), laminin, and fibronectin—in DCM and IHD tissue cross-sections. Here, we found the muscle fiber honeycomb geometry typical of healthy heart tissues was deranged in pathological heart and showed increased ECM structural protein deposition and distribution (Figure 1F), as also demonstrated in MI mice.[7] Finally, we quantified total collagen in healthy and diseased human hearts by hydroxyproline method and found that both DCM and IHD tissues displayed an increase in collagen composition (2.4-fold and 3.6-fold, respectively), compared with healthy controls. The increase was only significant in IHD (Figure 1G). We confirmed the loss of tissue integrity (Figure 1H) and ECM protein rearrangement (Figure 1I) in acute and chronic MI murine heart tissue (Online Figure IB).

These results demonstrate that reduced cardiac function in human HF is mirrored at the microscale by the derangement of tissue functional architecture and rearrangement of ECM structural proteins.

Decellularization Confirms ECM Microstructure and Biochemical Changes During Heart Disease

To highlight specific modifications in cardiac ECM microstructure during HF, we decellularized DCM and IHD patient cardiac samples, adapting a protocol described in fetal and adult murine hearts.[14,15] Masson's trichrome staining of dECMs confirmed the histological derangements observed in DCM and IHD ECM tissue geometry were preserved after decellularization (Figure 2A). Collagen I, IV, laminin, and fibronectin staining in dECMs showed structural disorganization and accumulation consistent with that observed in nondecellularized ECM (Figure 2B). Similarly, collagen composition also increased in DCM and IHD dECMs by ≈2-fold compared with healthy hearts (Figure 2C), mirroring the trend found in nondecellularized ECMs (Figure 1G). Finally, mass spectrometry analysis of ECM-associated proteins corroborated a marked shift in ECM composition in both pathological samples compared with healthy dECMs, with increased collagen, glycoprotein, and proteoglycan content (Figure 2D). In particular, DCM dECMs showed increased fibrinogen, fibrin, and collagen I, IV, and VI content, while IHD dECMs had enhanced TGFβ1, most of the Lamins, Hspg2, Collagen I, IV, and VI, Tgm2, and Cilp. While our mass spectrometry results on DCM dECM confirm and extend previous findings,[18] IHD data align with the ECM alterations reported in murine models of ischemia,[7] and in our chronic MI mouse dECM samples (Figure 2E).

Altogether, these results indicate that cardiac ECM decellularization is a suitable approach to investigate changes in cardiac ECM microstructure and biochemistry during HF.

ECM Organizational Complexity and Elasticity Is Reduced in HF

After confirming that decellularization allows for a comprehensive description of specific biochemical and structural changes in human HF, we focused on detailed pathological features in decellularized cardiac ECM.

Surface topography analysis performed by scanning electron microscopy revealed healthy human dECM displayed a characteristic structure defined by wavy fiber bundles. In DCM, however, surface topography was mildly disrupted or disconnected, while in IHD the structure was severely remodeled with a flat and compact appearance (Figure 3A). We also detected the loss of perimysial-like fibers and their replacement by a compact structure comprising straight fibers in human HF dECMs (Figure 3A). Image analysis of pathological dECM surface topography revealed an increase in structural coherence (between 6- and 18-fold) with acquisition of a dominant fiber direction (between 1.3- and 4-fold; Figure 3B). These features were also detected in chronic murine MI (Figure 3C and 3D).

We next used 2-photon microscopy to resolve the 3D arrangement of collagen fibers within dECMs by exploiting the second harmonic generation (SHG) phenomenon. Upon 3D reconstruction, DCM displayed a disintegrated collagen mesh that contrasted with IHD dECM, which rather showed a compact and stratified fiber distribution (Figure 3E, Online Movies I through III). Also, the derangement of the highly interconnected fibers of the healthy dECM led to matrix complexity loss, as shown by a clear reduction in SHG signal in both pathological dECMs, which was only significant in DCM (Figure 3F). As the remodeled ECM is characterized by fiber rearrangement, we reasoned this change might interfere with its elastic properties.

We thus used atomic force microscopy to locally measure the elasticity of healthy and diseased human dECMs: we found DCM and IHD dECMs to have a significantly lower (3-fold) Young's modulus than the healthy dECMs (Figure 3G), indicative of reduced elasticity and lower resistance to deformation. The analysis of a noncontractile scar in chronic MI in rodents, which has been associated with stiffening of the left ventricle[7] correlated with an increased signal of SHG (Figure 3H and 3I; Online Movie IV).

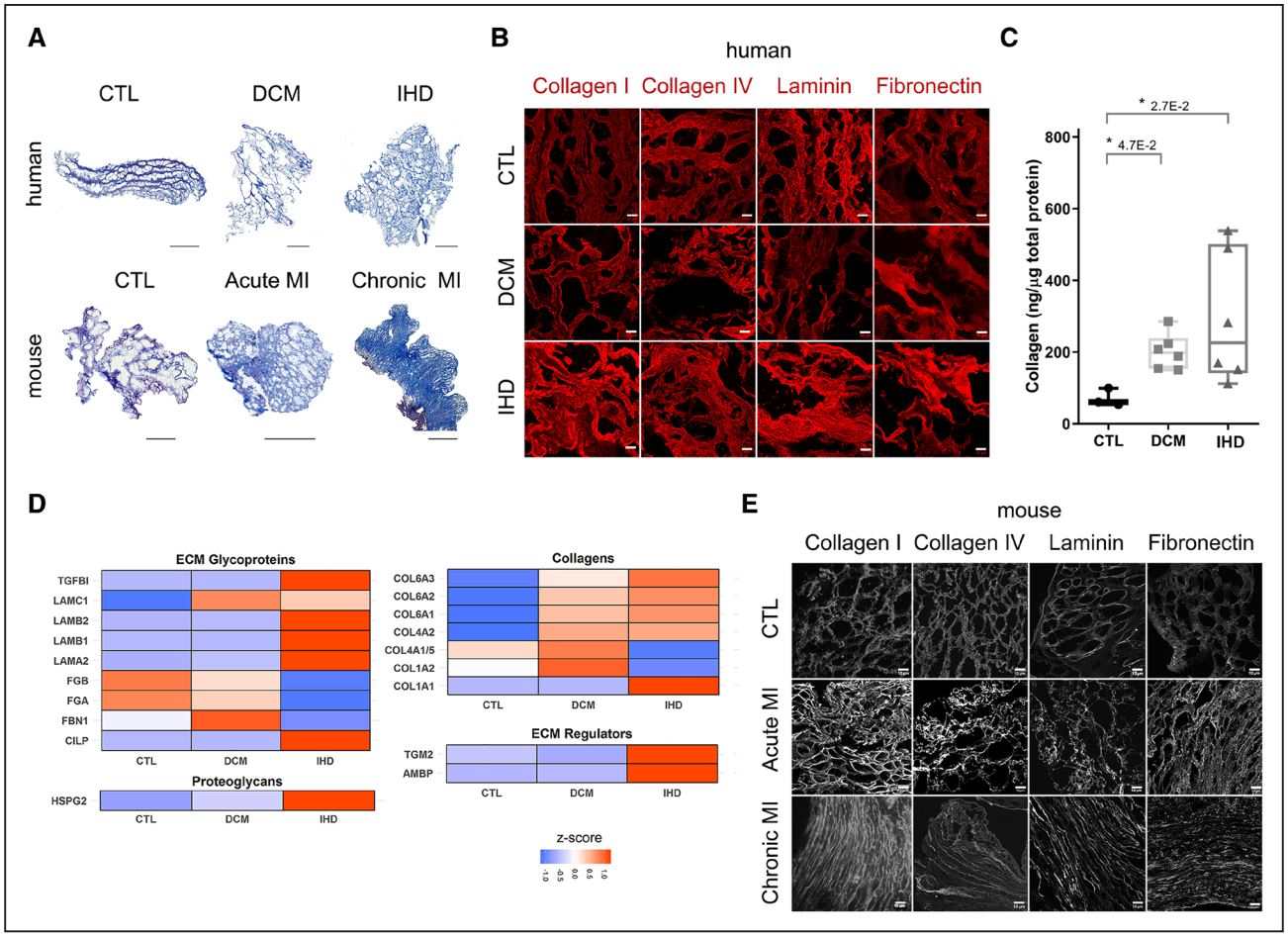

Figure 2. ECM (extracellular matrix) decellularization as a tool to analyze biochemical and structural ECM changes in human cardiac pathologies.

A, Representative Masson's trichrome staining of decellularized ECMs (dECMs) derived from healthy (CTL), dilated cardiomyopathy (DCM), and ischemic heart disease (IHD) human hearts (top) and CTL (sham-operated), acute and chronic infarcted (myocardial infarction [MI]) murine hearts (bottom). Scale bar=200 µm. **B**, Representative confocal microscopy images of the indicated ECM proteins in dECM obtained from CTL, DCM, and IHD patients. Scale bar=10 µm. **C**, Quantification of total collagen in dECMs obtained from CTL, DCM, and IHD human specimens. CTL (N=3; n=2), DCM (N=6; n=3), IHD (N=6; n=3); Kruskal-Wallis followed by Dunn's tests. Boxplots represent median±min/max. **D**, Heatmap representation of MS analysis of dECM from CTL, DCM, and IHD human specimens. CTL (n=3), DCM (n=3), IHD (n=6). **E**, Representative confocal images of the indicated ECM structural components in dECM obtained from CTL, acute and chronic MI mouse hearts. Scale bar=10 µm. See MS data analysis in the Data Supplement. TGFβ1 indicates transforming growth factor β 1.

Overall, we found that pathological ECM encompasses a severe rearrangement of collagen fibers, loss of ECM structural complexity and organization, eventually leading to reduced ECM elasticity.

ECM Remodeling During HF Impairs Cell Homing

Alongside the elastic and structural roles, ECM also provides homing to cardiac cells and guidance to circulating cell populations. Recent attempts to improve deteriorating heart function by implanting healthy cells with contractile potential have generated unsatisfactory results.[19] These outcomes have been ascribed to the hostile microenvironment of the diseased ECM preventing cells from homing and engrafting,[20–22] through debated mechanisms.[21,23] Here, we asked whether the rearrangement of ECM nanofibers observed in diseased heart tissues affected cell homing.

We developed a 3D CFD simulation to estimate the diffusion of a fluid through the dECMs, starting from SHG images. The surface tortuosity tensor readout describes the accessibility of the ECM and represents a precise characterization of the geometric properties and spatial orientation of dECM fibers in human HF. The workflow adopted is shown in Online Figure II. We evaluated the porosity, anisotropy (directional dependence), and connectivity of SHG structures using a recently developed method that considers connectivity factors as the inverse of the tortuosity.[24] Representative color-coded images of concentration profiles from which the surface tortuosity tensor was evaluated showed that, while the concentration profile of diffusive surface tortuosity was relatively uniform in healthy dECM, an emergence of a prevalent 3D fiber

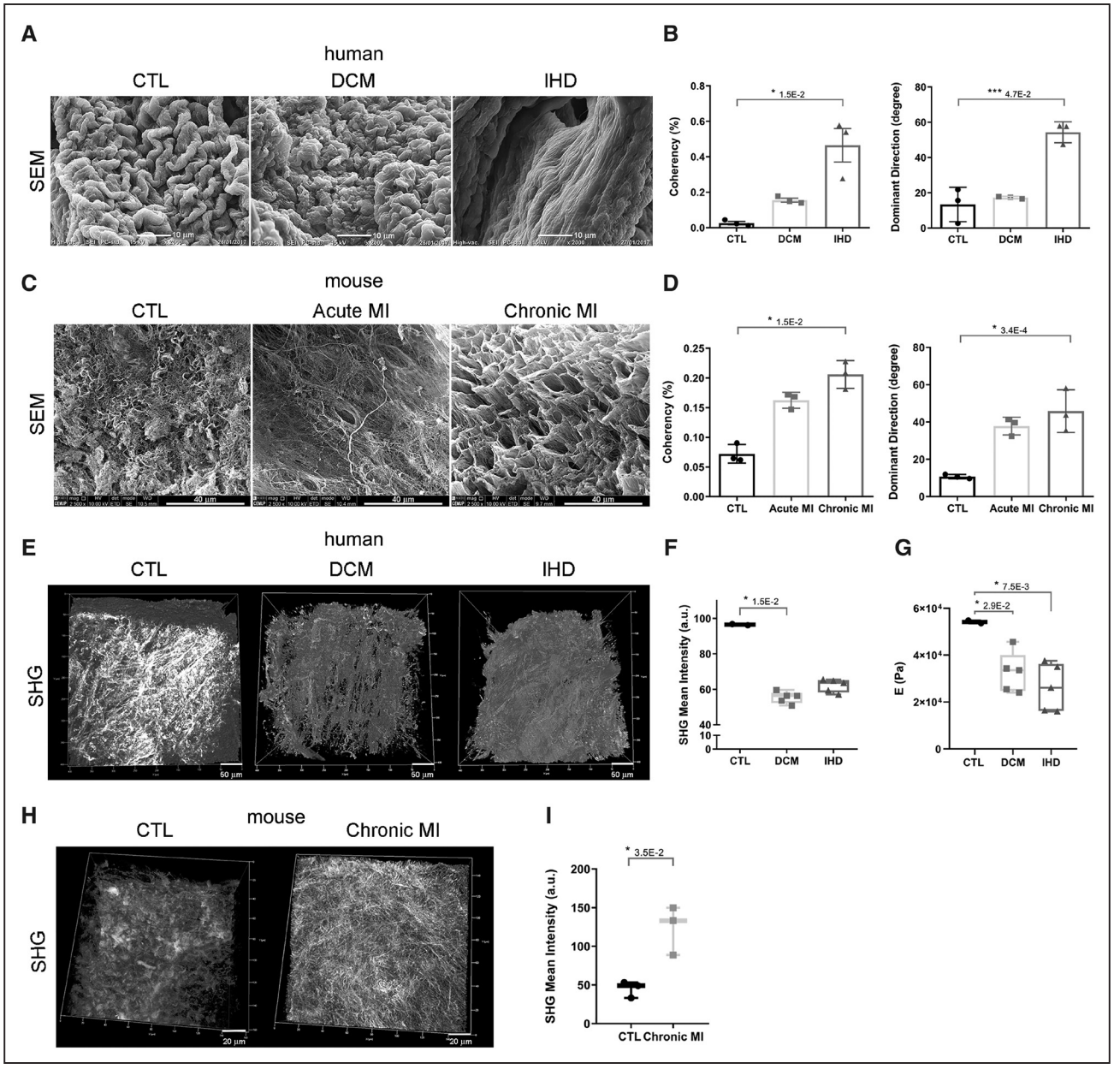

Figure 3. Decellularized ECMs (dECMs) from failing hearts show reduced ECM (extracellular matrix) complexity and elasticity. **A**, Representative images of dECM surface topography in healthy (CTL), dilated cardiomyopathy (DCM), and ischemic heart disease (IHD) human hearts mapped by scanning electron microscopy (SEM). **B**, Quantification of surface microstructure coherence (left) and fiber orientation (right) of the indicated dECMs (N=3; n=2); Kruskal-Wallis followed by Dunn's tests. **C**, Representative images of dECM surface topography in CTL (sham-operated), acute or chronic infarcted (myocardial infarction [MI]) murine hearts. **D**, Quantification of dECM fiber coherence (left) and fiber orientation (right) in dECMs obtained from CTL, acute, and chronic MI. CTL (N=3; n=6); acute, chronic MI (N=3; n=4). Kruskal-Wallis followed by Dunn tests. **E**, Three-dimensional (3D) reconstruction of CTL, DCM, and IHD human hearts produced by second harmonic generation (SHG) using 2-photon microscopy. **F**, Quantification of the SHG signal produced by healthy and pathological human dECMs. CTL (N=2; n=3), DCM, IHD (N=5; n=3); Kruskal-Wallis followed by Dunn tests. **G**, Quantification of the elasticity (Young's Modulus) of human healthy and pathological dECM by atomic force microscopy. CTL (N=2; n=5), DCM (N=5; n=6), IHD (N=5; n=8); Kruskal-Wallis followed by Dunn tests. **H**, Representative 3D images of CTL and chronic MI murine dECMs produced by 2-photon microscopy. **I**, Quantification of the SHG signal produced by murine dECMs (N=3; n=3). Mann-Whitney *U* test. Boxplots represent median±min/max and barplots represent mean±SD. A.u. indicates arbitrary units.

orientation (represented in eigen values) and tortuosity could be found in both DCM and IHD dECMs, being more pronounced in the latter condition (Figure 4A). These data mean the degree of collagen alignment in HF ECM tends to increase, indicating adverse collagen remodeling or scar development. Indeed, 3D segmentation followed by CFD simulations identified a 25-fold reduction in DCM specimen internal porosity. The decrease was not significant in IHD, possibly due to sample heterogeneity (Figure 4B). This analysis provided evidence that the enrichment in fibers with a dominant direction led to an increment in overall anisotropy (Figure 4C). These deviations in myocardial

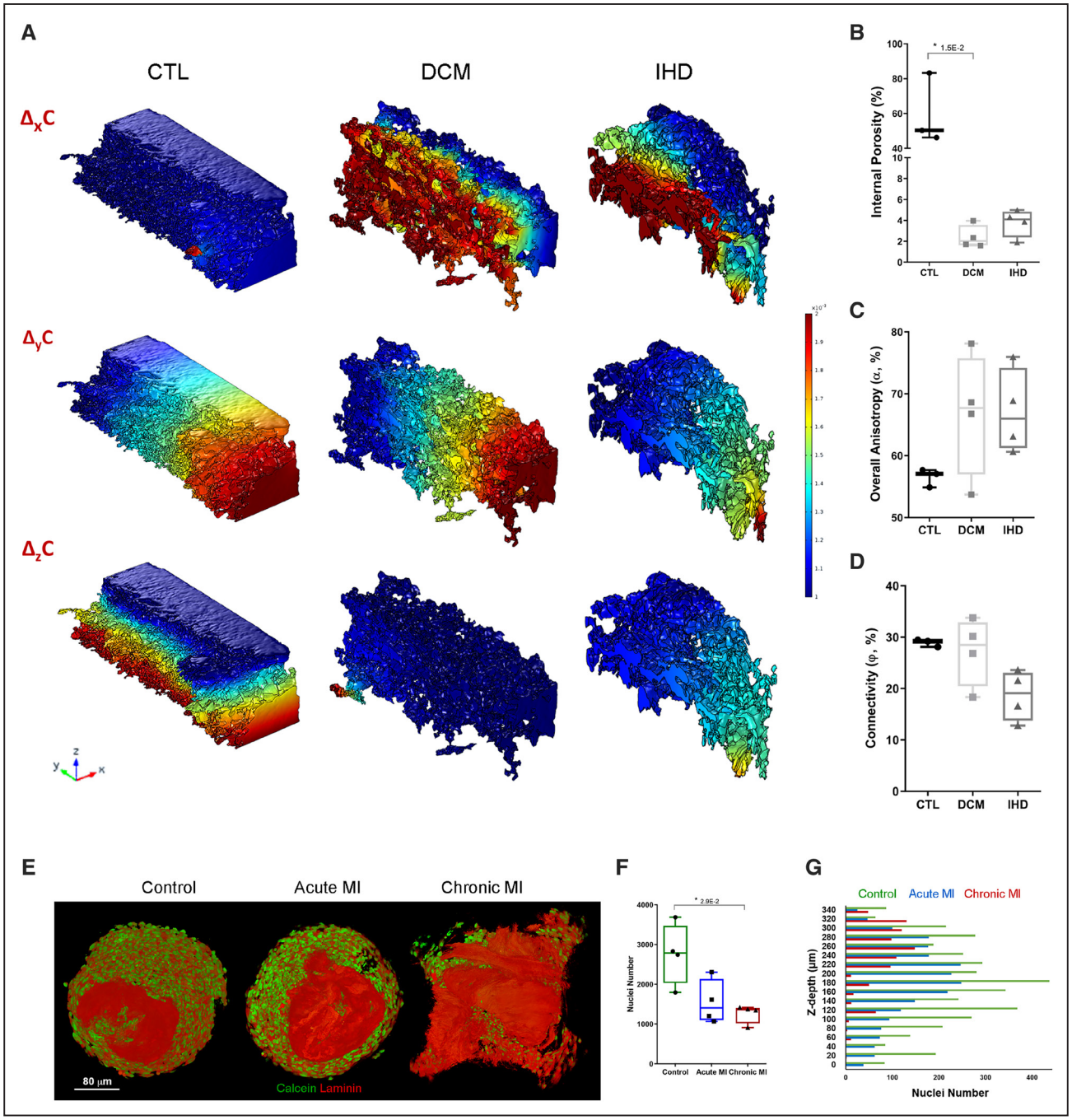

Figure 4. ECM (extracellular matrix) remodeling in heart failure reduces interconnected porosity and impairs cell homing. **A**, Representative color-coded images of concentration profiles of diffusive surface tortuosity obtained by 3-dimensional (3D) computational fluid dynamics simulation of healthy (CTL), dilated cardiomyopathy (DCM), and ischemic heart disease (IHD) decellularized ECMs (dECMs). **B**–**D**, Boxplot representation of porosity, anisotropy, and connectivity in CTL, DCM, and IHD human dECMs. CTL (N=3; n=2), DCM, IHD (N=4; n=2); Kruskall-Wallis test followed by Dunn tests. **E**, Representative 3D images obtained by 2-photon microscopy of human cardiac fibroblasts (CFs) cultured for 7 d within mouse CTL, acute or chronic infarcted (myocardial infarction [MI]) dECMs. dECM is stained with laminin (red), and cells are stained with calcein-AM live dye (green). **F**, Quantification of the total CFs population colonizing CTL, acute MI or chronic MI dECMs. Boxplots represent median±min/max. **G**, Layer-by-layer quantification of CFs colonization, and distribution in CTL (green), acute MI (blue), or chronic MI (red) dECMs. N=4; Kruskall-Wallis test followed by Dunn tests.

fiber anisotropy are credited of promoting changes in heart polarity that compromise electrical conduction.[25,26] Finally, we calculated the interconnected porosity of dECMs as an inverse function of tortuosity/anisotropy and observed a tendency toward reduced interconnected porosity in pathological dECMs (10% reduction, Figure 4D). This result is consistent with lower transport of both nutrients and metabolic products in pathological hearts.

To determine the consequences of reduced interconnected porosity and enhanced anisotropy on cell-ECM interaction, we cultured human CFs for 7 days on dECMs obtained from sham-operated, acute, and chronic MI murine hearts.[23,27] We predicted that this approach would help us isolate the contribution of the remodeled cardiac ECM on cell repulsion in the absence of immune response at early and late phases post-MI.

One week after seeding, we tracked the cells in the dECMs by incubating them with live dye Calcein-AM, while decorating for Laminin expression to visualize dECM structure (Figure 4E). Cell quantification within the dECMs indicated that CFs preferentially homed to the sham-operated dECMs, while a lower number (2-fold) of cells were found in acute and chronic MI (Figure 4F). Layer-by-layer analysis of cell distribution confirmed CFs failed to penetrate the inner core of the matrices derived from ischemic hearts (Figure 4G; Online Movies V through VII).

Altogether, these results suggest the reduced internal porosity and connectivity associated with cardiac ECM pathological remodeling has a detrimental effect on cell homing to the pathological tissue.

DCM Patient-Derived CFs Display Higher Susceptibility to Be Activated By Remodeled ECM

Pathological ECM remodeling in the heart is governed by CFs acquiring the contractile myofibroblast phenotype. This process can be followed by the expression of α-SMA (α-smooth muscle actin).[2,28] In DCM heart, CFs displayed higher basal levels of α-SMA as compared with healthy tissue (Figure 5A). We, thus, isolated primary CFs from healthy and DCM tissues, which showed a homogeneous derangement in ECM structure. After selecting CD90+/CD31− cells, we imaged vimentin-positive cells (Online Figure IIIA) and confirmed their fibroblastic features by using brightfield and scanning electron microscopy (Figure 5B). Next, we searched for genes being differentially regulated in DCM as compared with healthy CFs by means of RNA sequencing (Figure 5B; Online Table IV), as a means to explain how cardiac fibroblasts orchestrate cardiac ECM remodeling. The analysis highlighted the regulation of 2396 genes in 2 distinct DCM patients (Figure 5C), which encode for specific collagen isoforms (*COL4A1*, *COL5A2, COL10A1*), molecules involved in ECM composition (*AGRN, CCBE1, HAS1, LAMA4, VEGFA)* and ECM homeostasis (*ADAM12*, *BMP2*, *TIMP2*). Among the genes whose expression underlies pathological ECM remodeling, we also found increased expression of master regulators of tissue inflammation and disease progression (*IL6, IL33, C3, INHBA, TNC, FGF2, NAMPT*), as well as adhesion molecules and ECM receptors (*GJA1, ITGA11, ITGB3, TUBA4A*; Figure 5D).

To overcome patient variability, we tracked the common regulated genes among 2 DCM patient CFs (DCMA, DCMB) that shared a common molecular annotation for ECM organization, which was associated with the regulation of known pathophysiological pathways such as TGFβ1, interleukin-1, TNF-alpha, and BDNF signaling (Figure 5E; Online Tables V and VI). Selected genes found regulated in RNA-seq were validated by RT-qPCR analysis (Online Figure IIIB). Although confirming the involvement of these signaling axes would need further experiments, these results indicate potential known and novel players in ECM remodeling.

Next, we confirmed that DCM CFs expressed higher levels of α-SMA than CTL in vitro (Figure 5F) and further stimulated them with TGFβ1, a central mediator of fibrosis, to test whether cells from healthy or pathological heart would be susceptible to fibrogenic stimuli. When stimulated, CFs from patients with DCM were more prone to accumulate α-SMA than healthy CFs (Figure 5G; Online Figure IIIC).

The mechanical and biochemical modifications associated with the cardiac ECM remodeling determine a feed-forward positive loop, which sustains CFs activation and differentiation to foster ventricular repair.[2,28] We asked whether the sustained activation of CFs found within the DCM environment was the result of the changes occurring in the biochemistry or in the microstructure of remodeling ECM. Therefore, we used healthy and pathological (DCM) dECM either to prepare 2-dimensional coating or as 3D scaffolds for CTL CFs culture. FACS analysis showed CFs were indeed induced to express α-SMA when cultured on DCM coating, while a stronger effect was obtained when cells were grown onto 3D DCM matrices. These results suggested the rearrangement of the 3D structure of cardiac ECM plays a major role in CFs activation (Figure 5H).

Next, we searched for dysregulated proteins in DCM CFs that might help us highlight their response to ECM remodeling and also explain their role in cardiac ECM derangement. We, therefore, performed mass spectrometry analysis of DCM and CTL CFs protein composition. Bioinformatic analyses identified numerous proteins being consistently dysregulated in 3 different DCM patients, which belonged mainly to the focal adhesion compartment (Figure 5I and 5J, Online Figure IIID). We hence quantified focal adhesion number in CTL and DCM CFs and confirmed pathological cells displayed a significantly higher number of vinculin-rich spikes (Figure 5K).

These results suggest the derangement in DCM ECM induces a sustained activation of CFs.

YAP Activation in CFs Sustains ECM Remodeling During HF

Our group previously demonstrated that focal adhesion assembly is under the control of YAP transcriptional activity.[11] The protein is sensitive to cell-cell contact[29] and activated by ECM-generated mechanical signals.[9,30,31]

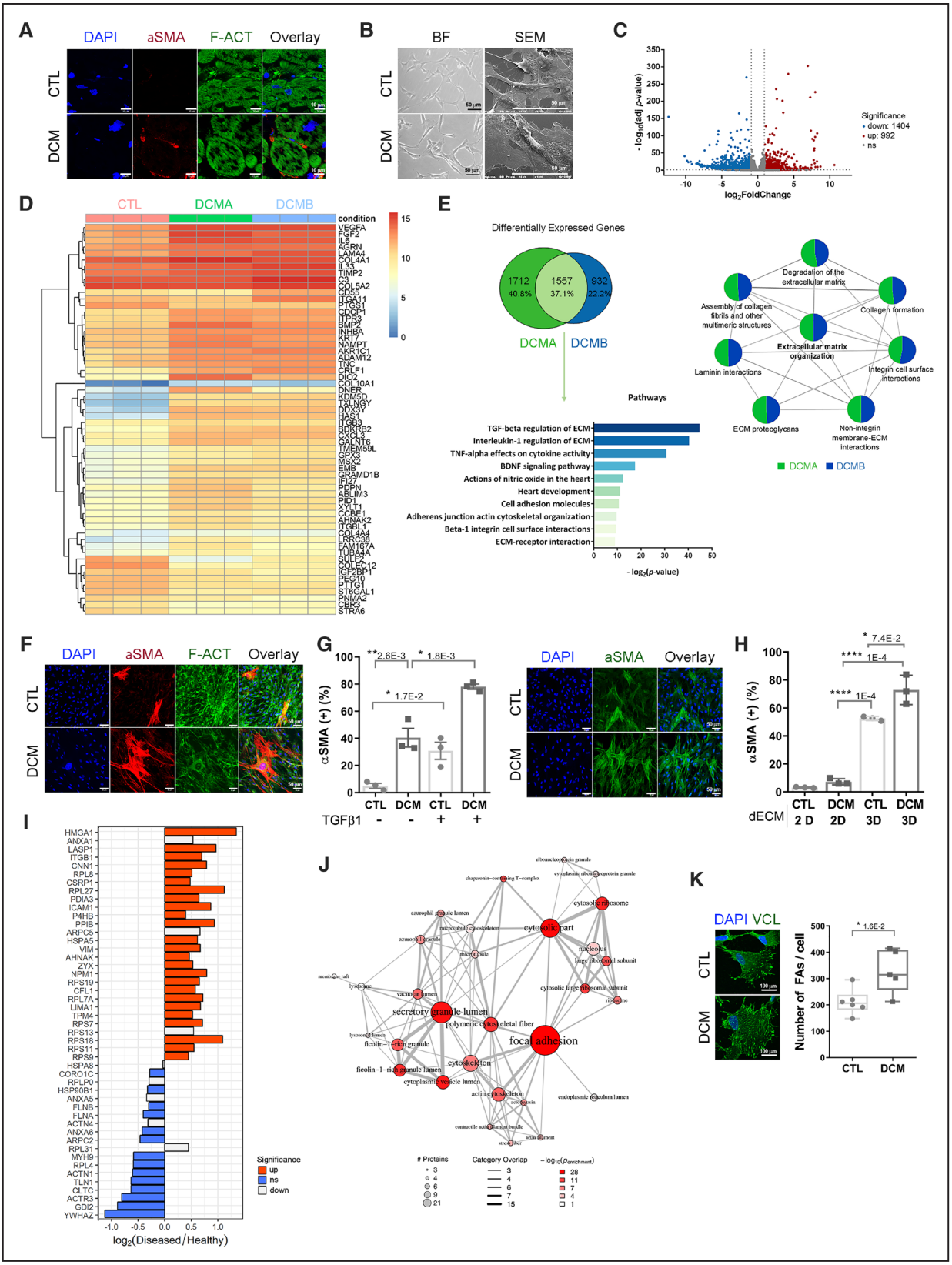

Figure 5. Human dilated cardiomyopathy (DCM) cardiac fibroblasts (CFs) express elevated levels of ECM (extracellular matrix) remodeling-associated molecules.

A, Representative confocal microscopy images depicting α-SMA (α-smooth muscle actin, red) expression in CTL and DCM heart tissues. **B**, Brightfield (BF) and scanning electron microscopy (SEM) images of CFs cultured from healthy (CTL) and DCM hearts. **C**, Volcano plot representation of the genes significantly regulated in DCM CFs (N=2) as compared with the same cells extracted from healthy (*Continued*)

Moreover, in adult heart, YAP is found exclusively expressed in CFs and endothelial cells, albeit being reactivated in cardiomyocytes after MI in mice[8,9] and in DCM and IHD in humans.[32] We, in fact, detected increased levels of YAP RNA in DCM heart tissue by RT-qPCR (Figure 6A) and confirmed the reexpression of the protein in both DCM CFs and cardiomyocytes in vivo by confocal microscopy (Figure 6B; Online Figure IVA).

To study YAP regulation in pathological heart, we generated mechanoreporter healthy and DCM CFs in which mCherry expression was under the control of YAP-TEAD transcriptional function[10] and detected a significantly higher reporter activity in DCM cells (1.3-fold; Figure 6C). This activity was confirmed by staining known YAP-TEAD target CTGF (connective tissue growth factor), being more expressed in DCM cells (Online Figure IVB).

We cultured healthy and DCM mechanoreporter CFs at low or high density and found YAP transcriptional activity to be repressed by cell-cell interactions (Figure 6D). Moreover, we seeded mechanoreporter cell lines on BiogelX-RGD or methacrylated gelatin substrates with controlled physiological stiffnesses and clarified YAP shuttling to the nucleus and YAP-TEAD transcriptional activity were indeed reinforced by substrate stiffening in both healthy and pathological cells (Figure 6E, Online Figure IVB).

Next, as 3D ECM features proved to be powerful in determining CFs maturation, we cultured the healthy mechanoreporter line on 2-dimensional and 3D DCM and CTL dECMs and found pathological matrix induced a significant enhancement (70%) in YAP-TEAD transcriptional activity (Figure 6F). These results indicated YAP-mediated mechanosensitive axis in CFs was responsive to modifications in cardiac ECM structure.

The interplay between Hippo and TGFβ1 signaling pathways is associated to the pathophysiology of fibrosis.[33] We thus stimulated healthy and DCM CFs with the same concentration of TGFβ1 able to induce α-SMA accumulation and found an increase in the expression of *YAP* gene. *CTGF* gene levels also tended to increase but were only significant in healthy CFs (Figure 6G).

Increased contractility is a characteristic of activated fibroblasts that can be measured by collagen contraction assay, a classic tool in the field of mechanobiology to study ECM cell-induced deformation. Therefore, we set up a contraction functional assay whereby we embedded healthy and DCM CFs in a collagen gel and quantified the ability of the cells to shrink the hydrogel by reshaping the collagen fibers. We found DCM CFs had significantly higher contractile activity compared with healthy CFs (Figure 6H). To investigate whether this increased contractility could be ascribed to the enhanced YAP–TEAD transcriptional activity, we generated CFs cell lines overexpressing the constitutively active nuclear form of YAP (YAP-8SA). YAP-8SA-overexpressing healthy CFs displayed increased ability to contract the collagen gels, while DCM CFs, which already displayed enhanced YAP activity, seemed to reach a plateau in their contraction capacity (Figure 6H). To confirm this result, we treated DCM and healthy CFs with YAP–TEAD complex inhibitor, verteporfin, and detected a reduced ability of DCM CFs to contract the collagen gel (Figure 6H).

Consistent with these results, RNA-seq analysis of common genes upregulated in YAP over-expressing and DCM CFs showed an overall rise in ECM organization annotation (*COL5A2*, *CTGF*, *FGF2*, *FBN1*, *LAMA2*, *TGFB2*) and membrane-ECM interactions (*ITGB1*, *ITGA11*) when compared with healthy CFs (Figure 6I, Online Figure IVC and IVD, Online Table VII). Remarkably, among the genes upregulated in YAP-overexpressing CFs, we found *ACTA2,* the gene encoding for α-SMA (Online Figure IVC).

These results indicate that pathological ECM remodeling during DCM could be because of YAP–TEAD hyperactivation in CFs.

DISCUSSION

Among the crucial challenges in cardiac tissue engineering is mimicking the structural complexity of ECM-cell interactions found in native tissue, as well as understanding how such complexity is perturbed with the onset of ischemic and chronic pathologies.[34] Cardiac remodeling entails the modification of ventricle 3D architecture as a result of myofibroblast activation and the consequent deposition of de novo synthesized noncompliant ECM.[35]

Figure 5 Continued. (CTL) heart as obtained by RNA-sequencing analysis. **D**, Heatmap representation of the top 60 differentially regulated genes in DCM and CTL CFs. **E**, Venn diagram representation of the differentially regulated genes from the patients with DCM—DCMA (green) and DCMB (blue)—and their common network of biological processes and pathophysiological pathways, obtained from Cytoscape software and ENRICHR database. **F**, Representative confocal microscopy images depicting α-SMA (red) expression in CTL and DCM CFs tissues. F-actin is stained with FITC-Phalloidin (green) and nuclei are counterstained with DAPI (4′,6-diamidino-2-phenylindole) (blue). **G**, FACS quantification (left) and representative confocal image (right) of α-SMA expression in CTL and DCM CFs treated or not with TGFβ (transforming growth factor β) for 72 h. N=3; ANOVA followed by Tukey test. **H**, FACS quantification of α-SMA expression in CTL CFs cultured for 48 h on (2-dimensional) or within (3-dimensional) decellularized ECM (dECM) generated from CTL and DCM heart tissues. N=3; ANOVA followed by Tukey test. **I**, Barplot representation of proteome profiling of the regulated proteins in DCM as compared with CTL CFs in mass spectrometry. **J**, Enrichment map of the regulated gene ontology cellular components in DCM compared with CTL CFs. Node size and font are proportional to the number of proteins identified in any given node; node color reflects the adjusted *P* value (Fisher exact test); the width of the edge is proportional to the overlap in proteins between connected categories; N=3. **K**, Representative confocal images and relative quantification of vinculin-rich (VCL, green) focal adhesions in CTL and DCM CFs. Nuclei are counterstained with DAPI (blue). CTL (N=6); DCM (N=5), Mann-Whitney *U* test. Boxplots represent median±min/max and barplots represent mean±SD. BDNF indicates brain derived neurotrophic factor; CTL, control; DAPI, 4′,6-diamidino-2-phenylindole; DCMA, DCM patient A; FA, focal adhesion; FACS, flow assisted cell sorting; F-act, F-actin; PECAM-1, platelet endothelial cell adhesion molecule 1; and RT-qPCR, reverse transcription quantitative polymerase chain reaction.

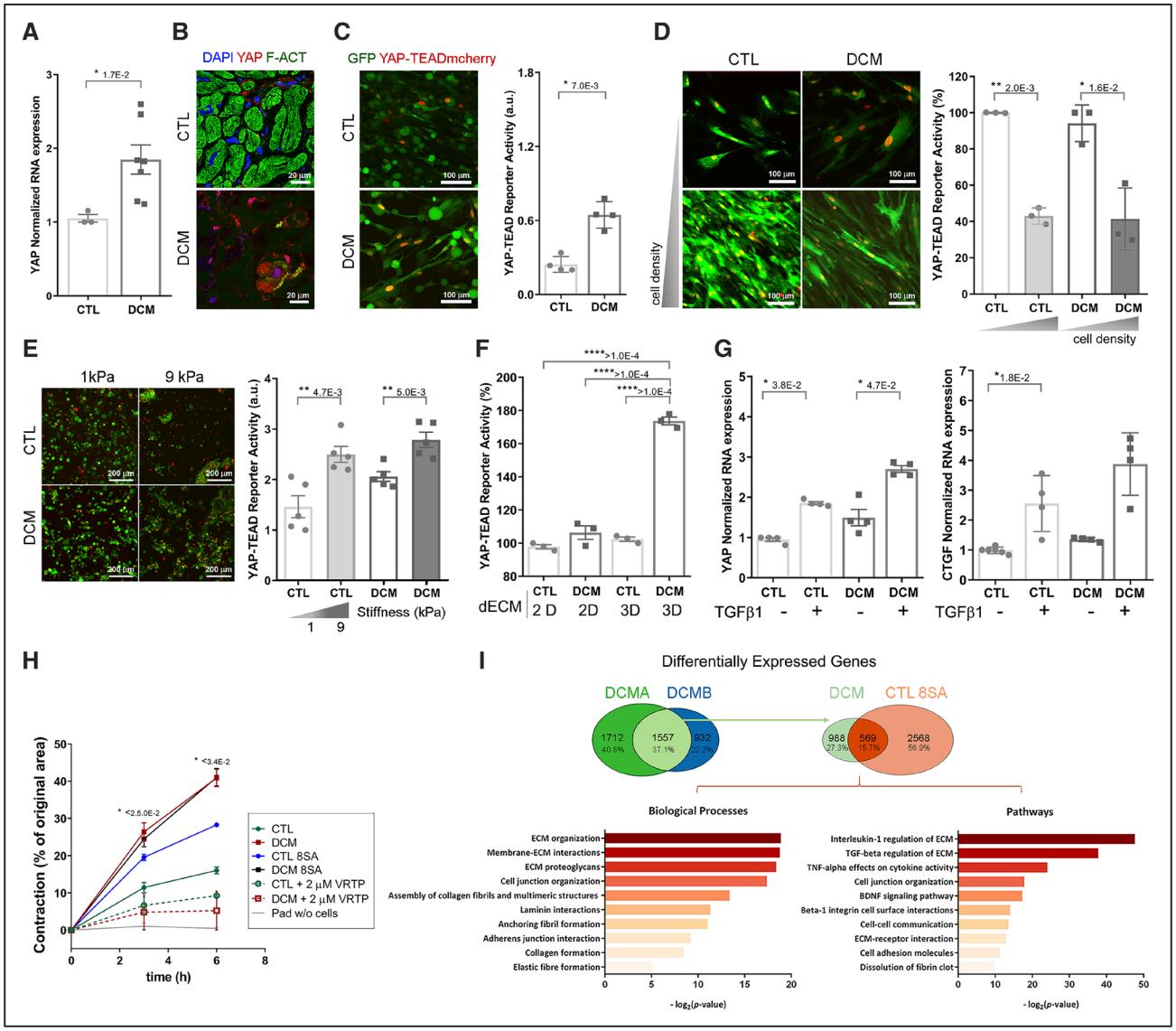

Figure 6. YAP (yes-associated protein) activation in dilated cardiomyopathy (DCM) cardiac fibroblasts (CFs) sustains ECM (extracellular matrix) remodeling during heart failure.

YAP RNA expression (**A**) and protein localization (**B**) in healthy (CTL) and dilated cardiomyopathy (DCM) hearts. CTL (N=3), DCM (N=7); Mann-Whitney *U* test. YAP (red), F-actin (green), nuclei (blue). **C**, Representative confocal image of YAP-transcriptional enhanced associate domain (TEAD) mechanoreporter lines obtained from DCM and CTL CFs and respective reporter activity. N=4; *t* test. **D**, Representative confocal image of the YAP-TEAD mechanoreporter line obtained from DCM CFs cultured under sparse and dense conditions (left) and the corresponding YAP-TEAD reporter activity (right). N=3; *t* test with Welch correction. **E**, Representative confocal images (left) and relative barplot representation (right) of YAP-TEAD reporter activity in CTL and DCM YAP-TEAD mechanoreporter cell lines cultured on BiogelX-RGD substrates with the indicated substrate stiffness. N=5. *t* test. **F**, Quantification of YAP-TEAD reporter activity in CTL CFs cultured for 48 h in 2-dimensional (2D) or 3-dimensional (3D) decellularized ECM (dECM) from CTL and DCM patients. N=3; ANOVA followed by Tukey test. **G**, RNA expression of YAP and CTGF in CTL and DCM CFs treated or not with TGFβ (transforming growth factor β) for 72 h; N=4; Kruskal Wallis followed by Dunn tests. **H**, Line graph representation of the ability of DCM and CTL CFs transfected or not with YAP-8SA plasmid, treated or not with 2 µmol/L of verteporfin (VRTP) to deform collagen at the indicated time points. The data are represented as the percentage of the original area of the pad that has been contracted by the cells. N=4; Kruskall-Wallis followed by Dunn test. *P* value refer to DCM vs CTL and DCM+VRTP vs DCM. **I**, Venn diagram representation of the genes found significantly regulated in both DCM CFs and in CTL-YAP-8SA compared with CTL, and respective barplot representation of common enriched gene ontology biological processes and pathways. Details of RNA sequencing data processing and statistics are shown in the Data Supplement. Boxplots represent median±min/max and barplots represent mean±SD.

Such remodeling presents as increased interstitial fibrosis and deranged geometric organization and integrity, resulting in conduction disturbances and reduced ejection fraction that eventually lead to HF.[35] While the biochemical changes associated with new ECM deposition have been extensively described in animal models,[36] the basis and impact of structural changes because of collagen assembly and alignment in human HF are poorly described.[34]

In this study, we combined scanning electron microscopy, atomic force microscopy and 3D 2-photon

microscopy imaging, with the aim of characterizing the alterations occurring in human cardiac ECM biophysical properties at end-stage HF. The samples were obtained from patients diagnosed with DCM or IHD and eligible for left ventricular assist device implantation or organ transplantation; the myocardium was treated by a decellularization protocol[14] that allowed preserving ECM geometry, mechanical properties, and biochemical features. By keeping into consideration that microscale assays might not fully extrapolate to the macroscale ECM heterogeneity of HF, we focused on the myocardium at the apical region of the left ventricle, which is affected by many cardiac dysfunctions, being detrimental for heart contractility, and a region of interest for noninvasive diagnosis. This strategy led us to highlight how ECM pathological remodeling is associated with a loss of complexity and helical structures, likely because of the deposition of aligned and compact fiber bundles displaying reduced local elasticity.

Although fibrotic conditions have been reported to increase bulk tissue stiffness,[26,36] here we analyzed the effective ECM rigidity after decellularization and by multimapping strategy to avoid region-specific biases and overcome sample heterogeneity. Therefore, different from well-established models of ischemia in which the scar region is measured, here we show that HF dECM softens and loses compliance in the absence of the cellular fraction or cellular forces contribution.

Next, we used 3D SHG high-resolution images of human heart dECMs as templates to feed an ad hoc designed CFD algorithm that computed the diffusion of a fluid through the matrices to generate a surface diffusive tortuosity tensor.[24] SHG is suited to monitor modifications to collagen network in vitro and in vivo. Indeed, researchers anticipated the use of noninvasive SHG coupled to magnetic resonance elastography as a strategy to follow-up vascularization or cardiac fibrosis and eventually lead to personalized treatments.[34,37,38] Our study shows a correlation between SHG signal and atomic force microscopy elastography and found a prevalent fiber orientation (increased anisotropy) in DCM and IHD dECMs, as compared with the more uniform and almost isotropic diffusive tortuosity of healthy dECMs. These anatomic differences contributed to reduce the interconnected porosity and make it a hostile environment, sufficient to hamper cell homing, in the absence of the immune response.

Altogether, we provide a comprehensive cardiac ECM atlas on the composition and structure of HF ECM templates, whose translational significance can be reflected into the following: (1) the identification of novel markers of cardiac dysfunction based on fine alterations of the cardiac ECM and (2) the definition of a rationale for the design of more effective antifibrotic cardiac regenerative strategies leading to personalized medicine. This includes the possibility of testing in vitro the downstream effects of ECM turnover, to address issues related to vascularization and attenuation of fibrosis, to study cardiomyocyte proliferation, CFs activation, and reactivation of innate immune mechanisms.

CFs and ECM integrity exist in a dynamic equilibrium, which is based on a feed-forward loop and altered during the progression of cardiac pathology. As CFs are key players in ECM remodeling[1,2] and fibrotic DCM is poorly understood,[39] we next obtained CFs lines from patients with DCM and performed genome-wide expression profiling and mass spectrometry to identify consistent changes in their gene and protein expression. We reasoned it would be possible by this means to correlate CFs phenotype with their ability to remodel cardiac ECM. The analysis led us to highlight that pathological CFs display altered expression of focal adhesion proteins and ECM-related genes. Indeed, functional analysis confirmed DCM cells more efficiently contract and deform collagen fibers than control cells and identified Hippo downstream effector YAP as a potent mediator of ECM pathological remodeling. YAP mechanosensitive protein, which is found reactivated in mouse MI[9] and in human DCM,[32] has been already associated with ECM remodeling[29–31] and connected to the acquisition of myofibroblast contractile phenotype.[13] Indeed, by generating CFs reporter cell lines of YAP transcriptional activity through TEAD, we showed DCM cells have sustained YAP expression and transcriptional activity and are more susceptible to differentiate into myofibroblasts. Consistently, YAP ectopic expression in healthy CFs leads them to the acquisition of a superior ability to contract ECM collagen fibers.

Additionally, we demonstrate the effectiveness of 3D ECM architecture in inducing CFs activation, regardless of biochemical cues. In extension to the axis of deterioration in HF (eg, inflammation, devascularization, demuscularization), our data suggest a crosstalk between TGFß1 and Hippo pathways, involving ECM and CFs. Together with the evidence that pathological CFs display hyperactive YAP–TEAD transcriptional axis, our data describe a feed-forward positive loop guided by YAP which sustains CFs activation and differentiation.

In conclusion, our results provide a comprehensive, high-resolution map of the modifications occurring in the collagen network organization during pathological cardiac ECM remodeling. We show that underlying this reorganization, the mechano-regulated YAP is activated in CFs to rearrange the ECM in a profibrotic feed-forward loop. These data, obtained from murine and human heart specimens, combine findings from medical records with in-depth multiparametric research outputs and functional assays, thus offering valuable preclinical information to future development of antifibrotic drugs and ultimate heart regenerative medicine approaches.

ARTICLE INFORMATION

Received June 19, 2020; revision received October 22, 2020; accepted October 25, 2020.

Affiliations

International Clinical Research Center, St. Anne's University Hospital Brno, Czech Republic (A.R.P., J.O.-D.L.C., F.M., V.H., G.C., O.P., V.V., S.P., K.K., G.F.). Instituto de Investigação e Inovação em Saúde and Instituto Nacional de Engenharia Biomédica, Universidade do Porto (A.C.S., P.P.-d.Ó., D.S.N.). Instituto de Ciências Biomédicas Abel Salazar, Universidade do Porto, Porto, Portugal (A.C.S., P.P.-d.Ó., D.S.N.). Gladstone Institute University of Cardiovascular Disease, San Francisco (A.C.S., J.O.-D.L.C.). Competence Center for Mechanobiology in Regenerative Medicine, INTERREG ATCZ133, Brno, Czech Republic (J.O.-D.L.C., F.M., V.V., G.F.). Faculty of Medicine, Department of Biology, Masaryk University, CZ-62500 Brno, Czech Republic (F.M.). Centre for Cardiovascular and Transplant Surgery, Brno, Czech Republic (V.H.). Central European Institute for Technology, Masaryk University, Brno, Czech Republic (G.C., P.S.). Department of Computer Engineering, Modelling, Electronics and Systems Engineering (G.A., A.C.) and Information Technology Center (G.d.M.), University of Calabria, Rende, Italy. First Institute of Pathological Anatomy, St. Anne's University Hospital Brno and Masaryk University, Brno, Czech Republic (V.Ž.). Università Campus Bio-Medico di Roma, Rome, Italy (A.R.). Department of Biomaterials Science, Institute of Dentistry, University of Turku, Finland (G.F.). Institute of Nanotechnologies (NANOTEC), National Research Council, Lecce, Italy (A.R.).

Acknowledgments

We thank Mrs Hana Dulova, Mrs Helena Ďuríková, Mrs Jana Bartoňová, Mrs Jana Vašíčková, Mrs Romana Vlckova, and Mrs Zuzana Travnicková (FNUSA-ICRC) for their technical assistance and the CKTCH physicians and nurses for their support in implementing this project. Dr Silvie Belaskova and the biostatistics and Mass Spectrometry Core Facilities of FNUSA-ICRC are gratefully acknowledged together with the Genomics and Bioinformatics Core Facilities of CEITEC Masaryk University for their support with data analysis and statistics. We also thank Dr Gaspar Pinto (Masaryk University, FNUSA-ICRC) for video editing and Insight Editing London for editing the article before submission.

Sources of Funding

This study was supported by the National Program of Sustainability II (MEYS CR; No. LQ1605), the study was also supported by the European Social Fund and European Regional Development Fund - Project MAGNET (No. CZ.02.1.01/0.0/0.0/15_003/0000492) and the Portuguese Foundation for Science and Technology (MatriCard; no. PTDC/SAU-ORG/118297/2010). Finally, we acknowledge CF Nanobiotechnology of CIISB, Instruct-CZ Centre, supported by MEYS CR (LM2018127).

Disclosures

None.

Supplemental Materials

Expanded Materials and Methods
Online Figures I–IV
Online Movies I–IV
Online Tables I–III
References[13–15,24,40–58]

REFERENCES

1. Nielsen SH, Mouton AJ, DeLeon-Pennell KY, Genovese F, Karsdal M, Lindsey ML. Understanding cardiac extracellular matrix remodeling to develop biomarkers of myocardial infarction outcomes. *Matrix Biol*. 2019;75-76:43–57. doi: 10.1016/j.matbio.2017.12.001
2. Talman V, Ruskoaho H. Cardiac fibrosis in myocardial infarction-from repair and remodeling to regeneration. *Cell Tissue Res*. 2016;365:563–581. doi: 10.1007/s00441-016-2431-9
3. Lindsey ML, Borg TK. Understanding the role of the extracellular matrix in cardiovascular development and disease: where do we go from here? *J Mol Cell Cardiol*. 2010;48:431–432. doi: 10.1016/j.yjmcc.2009.09.007
4. Evangelatov A, Pankov R. The evolution of three-dimensional cell cultures towards unimpeded regenerative medicine and tissue engineering. In: Andrades JA, ed. *Regenerative Medicine and Tissue Engineering*. InTech;2013:221–246.
5. Moroni F, Mirabella T. Decellularized matrices for cardiovascular tissue engineering. *Am J Stem Cells*. 2014;3:1–20.
6. Lynch M, Barallobre-Barreiro J, Jahangiri M, Mayr M. Vascular proteomics in metabolic and cardiovascular diseases. *J Intern Med*. 2016;280:325–338. doi: 10.1111/joim.12486
7. Sullivan KE, Quinn KP, Tang KM, Georgakoudi I, Black LD 3rd. Extracellular matrix remodeling following myocardial infarction influences the therapeutic potential of mesenchymal stem cells. *Stem Cell Res Ther*. 2014;5:14. doi: 10.1186/scrt403
8. Del Re DP, Yang Y, Nakano N, Cho J, Zhai P, Yamamoto T, Zhang N, Yabuta N, Nojima H, Pan D, et al. Yes-associated protein isoform 1 (Yap1) promotes cardiomyocyte survival and growth to protect against myocardial ischemic injury. *J Biol Chem*. 2013;288:3977–3988. doi: 10.1074/jbc.M112.436311
9. Mosqueira D, Pagliari S, Uto K, Ebara M, Romanazzo S, Escobedo-Lucea C, Nakanishi J, Taniguchi A, Franzese O, Di Nardo P, et al. Hippo pathway effectors control cardiac progenitor cell fate by acting as dynamic sensors of substrate mechanics and nanostructure. *ACS Nano*. 2014;8:2033–2047. doi: 10.1021/nn4058984
10. Oliver-De La Cruz J, Nardone G, Vrbsky J, Pompeiano A, Perestrelo AR, Capradossi F, Melajová K, Filipensky P, Forte G. Substrate mechanics controls adipogenesis through YAP phosphorylation by dictating cell spreading. *Biomaterials*. 2019;205:64–80. doi: 10.1016/j.biomaterials.2019.03.009
11. Nardone G, Oliver-De La Cruz J, Vrbsky J, Martini C, Pribyl J, Skládal P, Pešl M, Caluori G, Pagliari S, Martino F, et al. YAP regulates cell mechanics by controlling focal adhesion assembly. *Nat Commun*. 2017;8:15321. doi: 10.1038/ncomms15321
12. Calvo F, Ege N, Grande-Garcia A, Hooper S, Jenkins RP, Chaudhry SI, Harrington K, Williamson P, Moeendarbary E, Charras G, et al. Mechanotransduction and YAP-dependent matrix remodelling is required for the generation and maintenance of cancer-associated fibroblasts. *Nat Cell Biol*. 2013;15:637–646. doi: 10.1038/ncb2756
13. Nascimento DS, Valente M, Esteves T, de Pina Mde F, Guedes JG, Freire A, Quelhas P, Pinto-do-Ó P. MIQuant–semi-automation of infarct size assessment in models of cardiac ischemic injury. *PLoS One*. 2011;6:e25045. doi: 10.1371/journal.pone.0025045
14. Silva AC, Rodrigues SC, Caldeira J, Nunes AM, Sampaio-Pinto V, Resende TP, Oliveira MJ, Barbosa MA, Thorsteinsdóttir S, Nascimento DS, et al. Three-dimensional scaffolds of fetal decellularized hearts exhibit enhanced potential to support cardiac cells in comparison to the adult. *Biomaterials*. 2016;104:52–64. doi: 10.1016/j.biomaterials.2016.06.062
15. Silva AC, Oliveira MJ, McDevitt TC, Barbosa MA, Nascimento DS, Pinto-do-Ó P. Comparable decellularization of fetal and adult cardiac tissue explants as 3D-like platforms for in vitro studies. *J Vis Exp*. 2019;145:e56924. doi: 10.3791/56924
16. Jugdutt BI. Ventricular remodeling after infarction and the extracellular collagen matrix: when is enough enough? *Circulation*. 2003;108:1395–1403. doi: 10.1161/01.CIR.0000085658.98621.49
17. Duprez DA, Gross MD, Kizer JR, Ix JH, Hundley WG, Jacobs DR. Predictive value of collagen biomarkers for heart failure with and without preserved ejection fraction: multi-ethnic study of atherosclerosis. *J Am Heart Assoc*. 2018;7:e007885. doi: 10.1161/JAHA.117.007885
18. DeAguero JL, McKown EN, Zhang L, Keirsey J, Fischer EG, Samedi VG, Canan BD, Kilic A, Janssen PM, Delfín DA. Altered protein levels in the isolated extracellular matrix of failing human hearts with dilated cardiomyopathy. *Cardiovasc Pathol*. 2017;26:12–20. doi: 10.1016/j.carpath.2016.10.001
19. Gnecchi M. Cell therapy for heart regeneration: learning from the past to build a brighter future. *Stem Cells Transl Med*. 2018;7:702–704. doi: 10.1002/sctm.18-0126
20. Bertero A, Murry CE. Hallmarks of cardiac regeneration. *Nat Rev Cardiol*. 2018;15:579–580. doi: 10.1038/s41569-018-0079-8
21. Gerbin KA, Murry CE. The winding road to regenerating the human heart. *Cardiovasc Pathol*. 2015;24:133–140. doi: 10.1016/j.carpath.2015.02.004
22. Panahi M, Papanikolaou A, Torabi A, Zhang JG, Khan H, Vazir A, Hasham MG, Cleland JGF, Rosenthal NA, Harding SE, et al. Immunomodulatory interventions in myocardial infarction and heart failure: a systematic review of clinical trials and meta-analysis of IL-1 inhibition. *Cardiovasc Res*. 2018;114:1445–1461. doi: 10.1093/cvr/cvy145
23. Stevens KR, Murry CE. Human pluripotent stem cell-derived engineered tissues: clinical considerations. *Cell Stem Cell*. 2018;22:294–297. doi: 10.1016/j.stem.2018.01.015
24. Bellini S, Azzato G, Grandinetti M, Stellato V, De-Marco G, Sun Y, Caravella A. A novel connectivity factor for morphological characterization of membranes and porous media: a simulation study on structures of mono-sized spherical particles. *Appl Sci*. 2018;8:573.
25. Valderrábano M. Influence of anisotropic conduction properties in the propagation of the cardiac action potential. *Prog Biophys Mol Biol*. 2007;94:144–168. doi: 10.1016/j.pbiomolbio.2007.03.014
26. Richardson WJ, Clarke SA, Quinn TA, Holmes JW. Physiological implications of myocardial scar structure. *Compr Physiol*. 2015;5:1877–1909. doi: 10.1002/cphy.c140067
27. Nagaraju CK, Robinson EL, Abdesselem M, Trenson S, Dries E, Gilbert G, Janssens S, Van Cleemput J, Rega F, Meyns B, et al. Myofibroblast phenotype

and reversibility of fibrosis in patients with end-stage heart failure. *J Am Coll Cardiol*. 2019;73:2267–2282. doi: 10.1016/j.jacc.2019.02.049
28. Dupont S, Morsut L, Aragona M, Enzo E, Giulitti S, Cordenonsi M, Zanconato F, Le Digabel J, Forcato M, Bicciato S, et al. Role of YAP/TAZ in mechanotransduction. *Nature*. 2011;474:179–183. doi: 10.1038/nature10137
29. Forte G, Pagliari S, Ebara M, Uto K, Tam JK, Romanazzo S, Escobedo-Lucea C, Romano E, Di Nardo P, Traversa E, et al. Substrate stiffness modulates gene expression and phenotype in neonatal cardiomyocytes in vitro. *Tissue Eng Part A*. 2012;18:1837–1848. doi: 10.1089/ten.TEA.2011.0707
30. Martino F, Perestrelo AR, Vinarský V, Pagliari S, Forte G. Cellular mechanotransduction: from tension to function. *Front Physiol*. 2018;9:824. doi: 10.3389/fphys.2018.00824
31. Hou N, Wen Y, Yuan X, Xu H, Wang X, Li F, Ye B. Activation of Yap1/Taz signaling in ischemic heart disease and dilated cardiomyopathy. *Exp Mol Pathol*. 2017;103:267–275. doi: 10.1016/j.yexmp.2017.11.006
32. Grannas K, Arngården L, Lönn P, Mazurkiewicz M, Blokzijl A, Zieba A, Söderberg O. Crosstalk between Hippo and TGFβ: subcellular localization of YAP/TAZ/Smad complexes. *J Mol Biol*. 2015;427:3407–3415. doi: 10.1016/j.jmb.2015.04.015
33. Spinale FG, Frangogiannis NG, Hinz B, Holmes JW, Kassiri Z, Lindsey ML. Crossing into the next frontier of cardiac extracellular matrix research. *Circ Res*. 2016;119:1040–1045. doi: 10.1161/CIRCRESAHA.116.309916
34. Konstam MA, Kramer DG, Patel AR, Maron MS, Udelson JE. Left ventricular remodeling in heart failure: current concepts in clinical significance and assessment. *JACC Cardiovasc Imaging*. 2011;4:98–108. doi: 10.1016/j.jcmg.2010.10.008
35. Spinale FG. Myocardial matrix remodeling and the matrix metalloproteinases: influence on cardiac form and function. *Physiol Rev*. 2007;87:1285–1342. doi: 10.1152/physrev.00012.2007
36. Aguirre AD, Vinegoni C, Sebas M, Weissleder R. Intravital imaging of cardiac function at the single-cell level. *Proc Natl Acad Sci U S A*. 2014;111:11257–11262. doi: 10.1073/pnas.1401316111
37. Jones JS, Small DM, Nishimura N. In vivo calcium imaging of cardiomyocytes in the beating mouse heart with multiphoton microscopy. *Front Physiol*. 2018;9:969. doi: 10.3389/fphys.2018.00969
38. Paweł R, Wiśniowska-Śmialek S, Wypasek E, Biernacka-Fijalkowska B, et al. Fibrosis of extracellular matrix is related to the duration of the disease but is unrelated to the dynamics of collagen metabolism in dilated cardiomyopathy. *Inflamm Res*. 2016;65:941–949. doi: 10.1007/s00011-016-0977-3
39. Jin B, Zhu J, Shi H-M, Wen Z-C, Wu B-W. YAP activation promotes the transdifferentiation of cardiac fibroblasts to myofibroblasts in matrix remodeling of dilated cardiomyopathy. *Braz J Med Biol Res*. 2018;52:e7914. doi: 10.1590/1414-431X20187914
40. Caluori G, Pribyl J, Pesl M, Oliver-De La Cruz J, Nardone G, Skladal P, Forte G. Advanced and rationalized atomic force microscopy analysis unveils specific properties of controlled cell mechanics. *Front Physiol*. 2018;9:1121. doi: 10.3389/fphys.2018.01121
41. Wiśniewski JR, Zougman A, Nagaraj N, Mann M. Universal sample preparation method for proteome analysis. *Nat Methods*. 2009;6:359–362. doi: 10.1038/nmeth.1322
42. Cox J, Neuhauser N, Michalski A, Scheltema RA, Olsen JV, Mann M. Andromeda: a peptide search engine integrated into the MaxQuant environment. *J Proteome Res*. 2011;10:1794–1805. doi: 10.1021/pr101065j
43. Cox J, Hein MY, Luber CA, Paron I, Nagaraj N, Mann M. Accurate proteome-wide label-free quantification by delayed normalization and maximal peptide ratio extraction, termed MaxLFQ. *Mol Cell Proteomics*. 2014;13:2513–2526. doi: 10.1074/mcp.M113.031591
44. R Core Team. R: A language and environment for statistical computing. In: *R Foundation for Statistical Computing*; 2018.
45. Merico D, Isserlin R, Stueker O, Emili A, Bader GD. Enrichment map: a network-based method for gene-set enrichment visualization and interpretation. *PLoS One*. 2010;5:e13984. doi: 10.1371/journal.pone.0013984
46. Costantini M, Testa S, Fornetti E, Barbetta A, Trombetta M, Cannata SM, Gargioli C, Rainer A. Engineering muscle networks in 3D gelatin methacryloyl hydrogels: influence of mechanical stiffness and geometrical confinement. *Front Bioeng Biotechnol*. 2017;5:22. doi: 10.3389/fbioe.2017.00022
47. Su S, Chen J. Collagen gel contraction assay. *Protoc Exch*. 2015.
48. Andrews S. FastQC: a quality control tool for high throughput sequence data. 2010. Available online at: https://www.bioinformatics.babraham.ac.uk/projects/fastqc/.
49. Bolger AM, Lohse M, Usadel B. Trimmomatic: a flexible trimmer for Illumina sequence data. *Bioinformatics*. 2014;30:2114–2120. doi: 10.1093/bioinformatics/btu170
50. Dobin A, Davis CA, Schlesinger F, Drenkow J, Zaleski C, Jha S, Batut P, Chaisson M, Gingeras TR. STAR: ultrafast universal RNA-seq aligner. *Bioinformatics*. 2013;29:15–21. doi: 10.1093/bioinformatics/bts635
51. Wang L, Wang S, Li W. RSeQC: quality control of RNA-seq experiments. *Bioinformatics*. 2012;28:2184–2185. doi: 10.1093/bioinformatics/bts356
52. Picard Toolkit. Broad Institute, GitHub Repository. 2018. Available online at: http://broadinstitute.github.io/picard/. Accessed July 9, 2020.
53. Okonechnikov K, Conesa A, García-Alcalde F. Qualimap 2: advanced multi-sample quality control for high-throughput sequencing data. *Bioinformatics*. 2016;32:292–294. doi: 10.1093/bioinformatics/btv566
54. Liao Y, Smyth GK, Shi W. featureCounts: an efficient general purpose program for assigning sequence reads to genomic features. *Bioinformatics*. 2014;30:923–930. doi: 10.1093/bioinformatics/btt656
55. Love MI, Huber W, Anders S. Moderated estimation of fold change and dispersion for RNA-seq data with DESeq2. *Genome Biol*. 2014;15:550. doi: 10.1186/s13059-014-0550-8
56. Zhang H, Tian L, Shen M, Tu C, Wu H, Gu M, Paik DT, Wu JC. Generation of quiescent cardiac fibroblasts from human induced pluripotent stem cells for in vitro modeling of cardiac fibrosis. *Circ Res*. 2019;125:552–566. doi: 10.1161/CIRCRESAHA.119.315491
57. Azzato G, De Marco G, Stellato V, Sun Y, Caravella A. Tortuosity and connectivity evaluation by CFD simulation for morphological characterization of membranes and catalytic structures. Case study: CaF2-like structure. *Chem Eng Sci*. 2019;195:519–530.
58. Caravella A, Hara S, Obuchi A, Uchisawa J. Role of the bi-dispersion of particle size on tortuosity in isotropic structures of spherical particles by three-dimensional computer simulation. *Chem Eng Sci*. 2012;84:351–371.